Electronic Supplementary Material (ESI) for Journal of Materials Chemistry C.
This journal is © The Royal Society of Chemistry 2023

Supporting Information

A Moldable PEDOT:PSS Dry Electrode with Excellent Epidermal Compliance for Wearable Electrocardiogram Monitoring

Xianglin Gao, Tong Su, Yilin Bao, Jipei Lu, Lei Zhang,*[a] Chaobin He[b, c], Jianyong Ouyang[b]

[a.] Department of Biomedical Engineering & Instrument Science, Key Laboratory for Biomedical Engineering of Ministry of Education, Zhejiang University, Hangzhou, 310027, China;

[b.] Department of Materials Science & Engineering, National University of Singapore, Singapore 117575, Singapore.

[c.] Institute of Materials Research and Engineering, Agency for Science Technology and Research (A*STAR), Singapore138634, Singapore.

***Correspondence to:** Lei Zhang, Department of Biomedical Engineering & Instrument Science, Key Laboratory for Biomedical Engineering of Ministry of Education, Zhejiang University, Hangzhou, 310027, China; Email: leimxi@zju.edu.cn

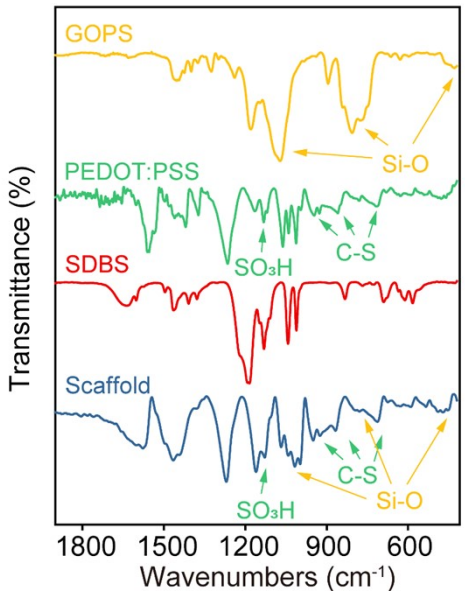

Figure S1. FT-IR spectra of raw materials and the PSG scaffold.

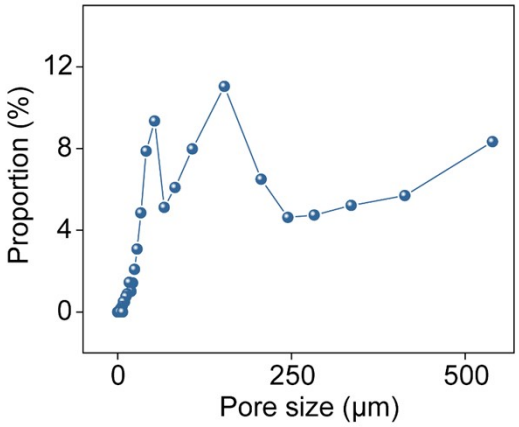

Figure S2. Pore sizes and distribution of PSG aerogel using mercury intrusion porosimetry.[1]

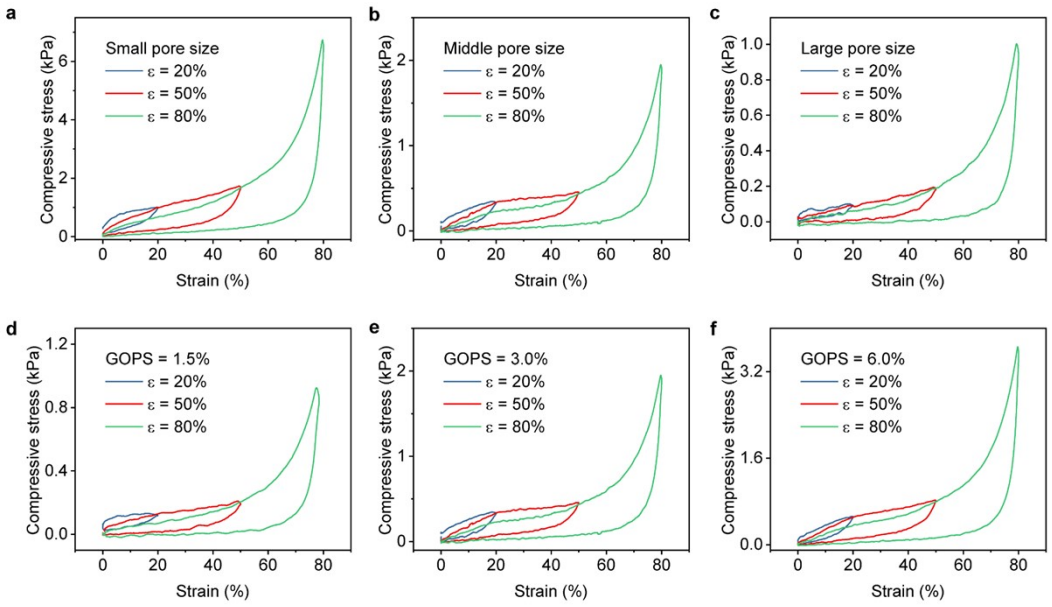

Figure S3. Stress-strain curves of the PSG electrodes with different pore sizes (a, b, c) and GOPS loading (d, e, f) under different compressive strains.

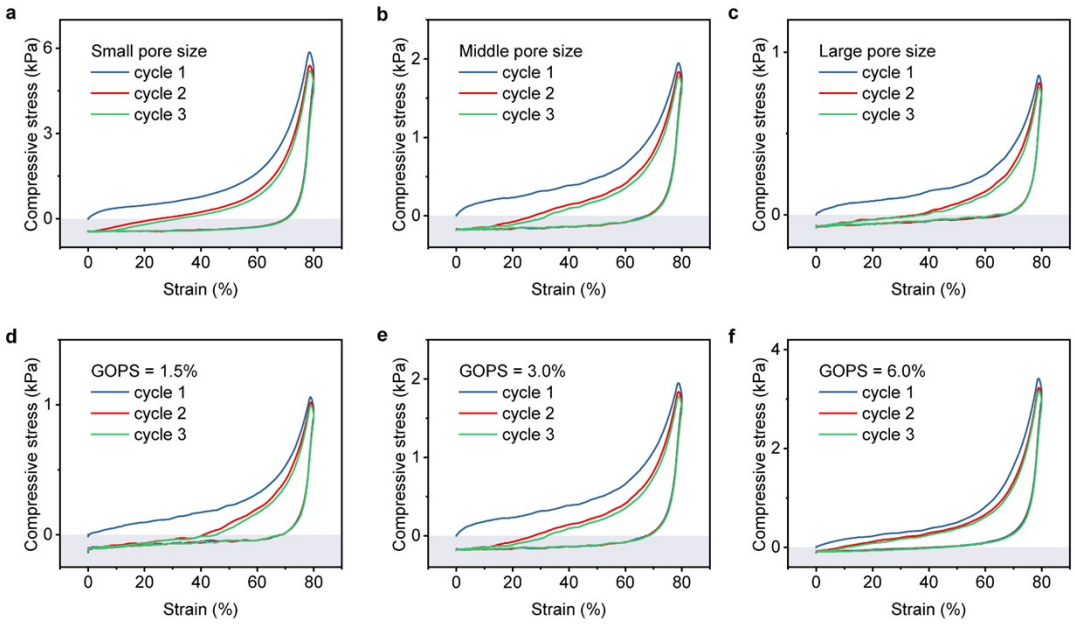

Figure S4. Three cycles of compression stress-strain curves of the PSG electrodes with different pore sizes (a, b, c) and GOPS loading (d, e, f) under 80% strain.

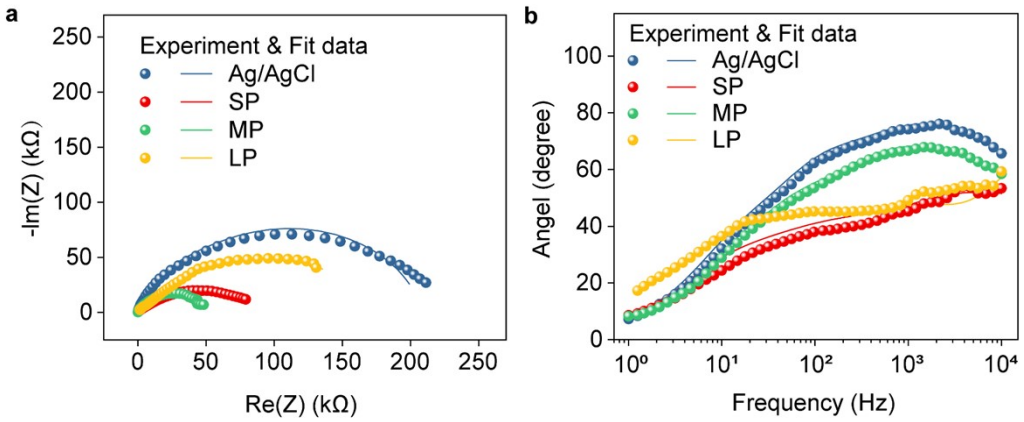

Figure S5. Nyquist plot (a) and Bode plot (b) obtained from the EIS characterization of PSG electrode with different pore size.

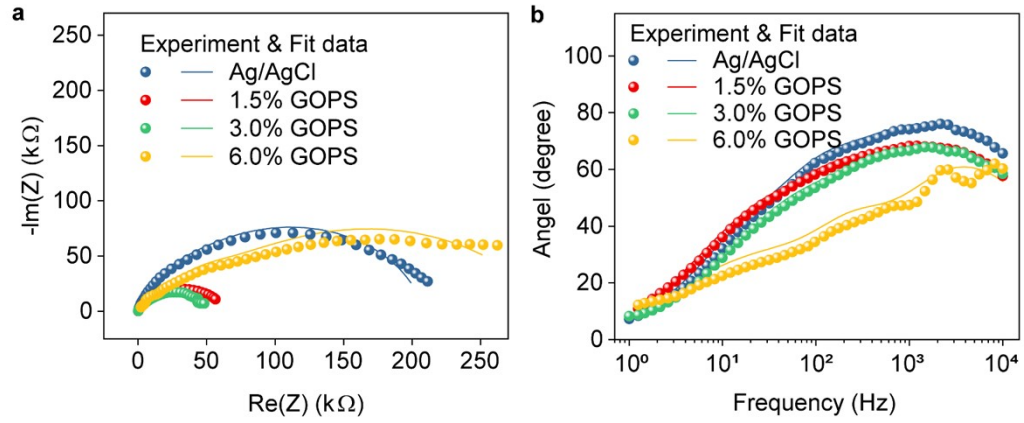

Figure S6. Nyquist plot (a) and Bode plot (b) obtained from the EIS characterization of PSG electrode with different GOPS loading.

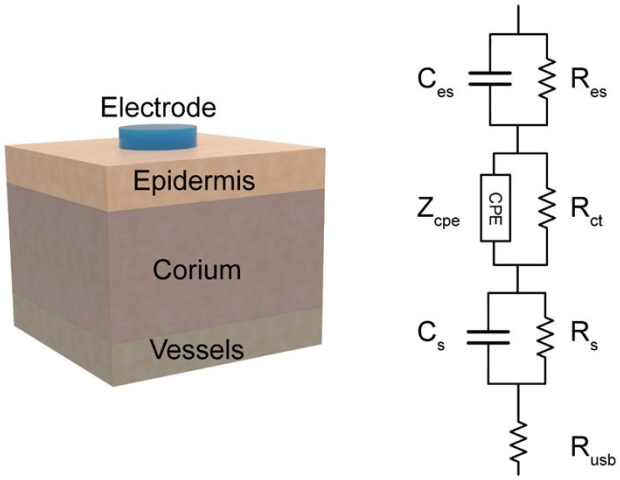

Figure S7. The equivalent circuit model of a PSG electrode attached on the skin.

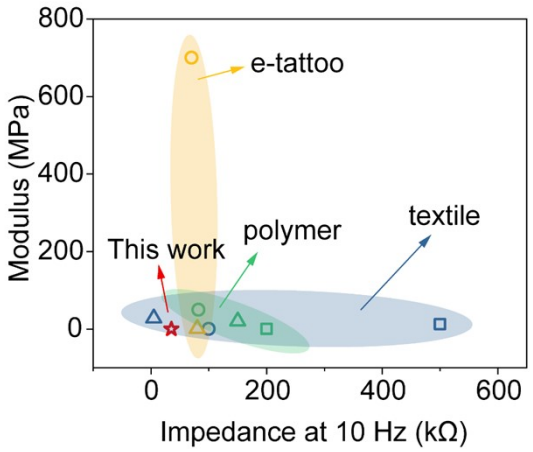

Figure S8. The comparation of PSG aerogel electrode in this work with other PEDOT: PSS based electrodes. The contact impedance and modulus of these electrodes are demonstrated in Supplementary Table S4.

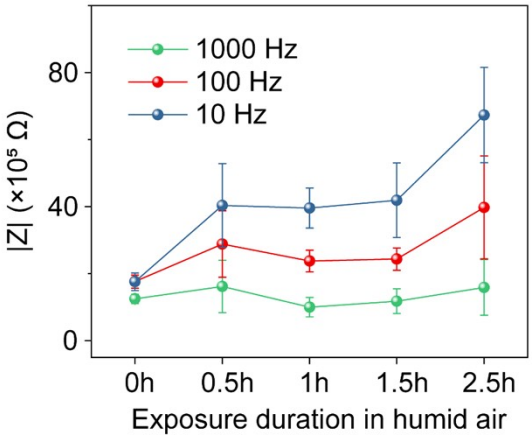

Figure S9. Impedances changes of the PSG scaffolds in 75% humidity air.

Table S1 Mechanical and electrical properties of freeze-dried PEDOT:PSS aerogels.

Aerogels No.	Modulus (kPa)	Conductivity (S/m)
PSG	1.71	1700
1[2]	95000	400
2[3]	80	1
3[4]	135000	49
4[5]	4.1	0.02
5[6]	48	0.00106

Table S2 The numerical fitting results of equivalent circuit components of Ag/Ag gel electrode and the PSG electrodes with different pore size.

	Ag/AgCl	SP	MP	LP
R_e (Ω)	2.69E+03	1.62E+04	7.50E+03	3.24E+03
C_{es} (F)	1.64E-08	1.56E-06	9.37E-05	7.22E-08
R_{ct} (Ω)	1.80E+05	6.50E+04	4.74E+04	1.74E+05
Q_{cpe} ($\Omega^{-1}\cdot cm^{-2}\cdot s^n$)	1.83E-07	1.16E-06	5.92E-07	6.51E-07
n_{cpe}	8.56E-01	5.81E-01	7.91E-01	6.58E-01
R_s (Ω)	2.63E+04	8.53E+02	1.54E+03	1.81E+03
C_s (F)	1.20E-07	1.41E-07	4.58E-07	1.06E-08
R_{usb} (Ω)	1.97E+02	7.36E+01	9.22E+01	1.01E-02

Table S3 The numerical fitting results of equivalent circuit components of Ag/Ag gel electrode and the PSG electrodes with different GOPS loading.

	Ag/AgCl	1.5% GOPS	3.0% GOPS	6.0% GOPS
R_e (Ω)	2.69E+03	2.57E+03	7.50E+03	2.93E+04
C_{es} (F)	1.64E-08	7.58E-07	9.37E-05	3.91E-08
R_{ct} (Ω)	1.80E+05	5.75E+04	4.74E+04	2.59E+05
Q_{cpe} ($\Omega^{-1}\cdot cm^{-2}\cdot s^n$)	1.83E-07	8.23E-07	5.92E-07	3.35E-07
n_{cpe}	8.56E-01	7.97E-01	7.91E-01	6.55E-01
R_s (Ω)	2.63E+04	4.33E+02	1.54E+03	1.23E+04
C_s (F)	1.20E-07	7.45E-07	4.58E-07	1.10E-08
R_{usb} (Ω)	1.97E+02	7.78E+01	9.22E+01	1.19E+03

Table S4 The contact impedance and modulus of some PEDOT:PSS based electrodes.

Electrode type	No.	Contact impedance* (kΩ)	Modulus (MPa)	SNR (dB)
PSG	This work	35.3	1.7×10^{-3}	22.54
Textile	1[7]	100	0.25	9.8
	2[8]	500	12.5	18.02
	3[9]	5	27.6	15.7
Polymer Blends	4[10]	200	0.1	18.9
	5[11]	82	50	18.1
	6[12]	150	20	11.4
E-tatoo	7[13]	70	700	19.9
	8[14]	80	0.64	18

* The skin-contact impedances at 10 Hz of the electrodes are compared.

Supplementary Note 1

To further investigate the electrical properties of PSG electrode, the electrochemical impedance spectroscopy (EIS) data were fitted to obtain the equivalent circuit model (as shown in Fig. S7).[15] In the model, the R_{es} represents the resistance of electrode and leads, and C_{es} represented the capacitance of electrode and epidermis. R_{ct} represents the charge transfer resistance and the constant phase element (Z_{cpe}) represented the geometric capacitance of contact interface,[16] which is used to account inhomogeneous or imperfect capacitance. The components of Z_{cpe} include peudo-capacitance (Q_{cpe}) and the deviation from ideal capacitive behavior (n).[17] The skin consisted of epidermal layer and corium layer, which could be modeled by R_s and C_s in parallel. The R_{usb} represented the resistance of other tissues or components (e.g. vessels) inside the skin.[18] The fitting results were illustrated in Fig. S5 and Fig. S6 The fitting parameters of equivalent circuit components of different electrodes are shown in supplementary Table S2 and Table S3, respectively.

It is demonstrated that the PSG electrode with middle pore size (MP) has significantly higher capacitance (C_{es}) and lower contact residence (R_{ct}) than the electrodes with small pore size and large pore size, which may attribute to the compliant contact between electrodes and skin. The adding of nonconducting GOPS will increase the residence of electrode (R_{es}). A moderate loading of GOPS at 3 wt% brings comparatively higher C_{es} and unsatisfactory resistance (R_{es}, R_{ct}). On the whole, the PSG electrode with middle pore size and 3 wt% GOPS shows the lowest contact impedance. On another hand, the optimal PSG electrode also shows significantly higher capacitance (C_{es}, 93.7 μF) and lower contact residence (R_{ct}, 47.4 kΩ) than that of Ag/AgCl gel electrode (C_{es}, 16.4×10^{-3} μF; R_{ct}, 180 kΩ), which gives rise to much lower contact impedance for high performance of ECG signal monitoring.

Supplementary Note 2

SNR is estimated according the formula below:

$$SNR = 20\lg\frac{V_{signal}}{V_{noise}}$$

where V_{signal} is the maximum variation of signal (RS wave of ECG signal) while V_{noise} is the maximum variation of noise in the ST wave band. [19-21]

Reference

1. Y. Zhu, R. Haghniaz, M. C. Hartel, S. Guan, J. Bahari, Z. Li, A. Baidya, K. Cao, X. Gao, J. Li, Z. Wu, X. Cheng, B. Li, S. Emaminejad, P. S. Weiss and A. Khademhosseini, *Adv. Mater.*, 2023, **35**, 2209300.
2. M. Dodel, N. Hemmati Nejad, S. H. Bahrami, M. Soleimani, L. Mohammadi Amirabad, H. Hanaee-Ahvaz and A. Atashi, *Biologicals*, 2017, **46**, 99-107.
3. I. del Agua, S. Marina, C. Pitsalidis, D. Mantione, M. Ferro, D. Iandolo, A. Sanchez-Sanchez, G. G. Malliaras, R. M. Owens and D. Mecerreyes, *ACS Omega*, 2018, **3**, 7424-7431.
4. C. Adler, M. Monavari, G. A. Abraham, A. R. Boccaccini and F. Ghorbani, *RSC Adv.*, 2023, **13**, 15960-15974.
5. G.-Y. Yang, S.-Z. Wang, H.-T. Sun, X.-M. Yao, C.-B. Li, Y.-J. Li and J.-J. Jiang, *ACS Appl. Mater. Interfaces*, 2021, **13**, 57521-57531.
6. M. A. Cassa, M. Maselli, A. Zoso, V. Chiono, L. Fracchia, C. Ceresa, G. Ciardelli, M. Cianchetti and I. Carmagnola, *Journal of Functional Biomaterials*, 2022, **13**, 135.
7. I. del Agua, D. Mantione, U. Ismailov, A. Sanchez-Sanchez, N. Aramburu, G. G. Malliaras, D. Mecerreyes and E. Ismailova, *Adv. Mater. Technol.*, 2018, **3**, 1700322.
8. Q. Li, G. Chen, Y. Cui, S. Ji, Z. Liu, C. Wan, Y. Liu, Y. Lu, C. Wang, N. Zhang, Y. Cheng, K.-Q. Zhang and X. Chen, *ACS Nano*, 2021, **15**, 9955-9966.
9. C.-Y. Huang and C.-W. Chiu, *ACS Appl. Electron. Mater.*, 2021, **3**, 676-686.
10. Y. Cheng, Y. Zhou, R. Wang, K. H. Chan, Y. Liu, T. Ding, X.-Q. Wang, T. Li and G. W. Ho, *ACS Nano*, 2022, **16**, 18608-18620.
11. L. Zhang, K. S. Kumar, H. He, C. J. Cai, X. He, H. Gao, S. Yue, C. Li, R. C.-S. Seet, H. Ren and J. Ouyang, *Nat. Commun.*, 2020, **11**, 4683.
12. L. Lan, F. Li, W. Li, R. Chen, Z. Xiong, Y. He, N. A. N. Ouedraogo, B. Ai, L. Tao, K. Sun and S. Chen, *ACS Appl. Mater. Interfaces*, 2022, **14**, 20113-20121.
13. Y. Chen, G. Zhou, X. Yuan, C. Li, L. Liu and H. You, *Biosens. Bioelectron.*, 2022, **206**, 114118.
14. Y. Zhao, S. Zhang, T. Yu, Y. Zhang, G. Ye, H. Cui, C. He, W. Jiang, Y. Zhai, C. Lu, X. Gu and N. Liu, *Nat. Commun.*, 2021, **12**, 4880.
15. K. Gao, H.-J. Yang, X. Wang, B. Yang and J. Liu, *Sens. Actuators, A*, 2018.
16. H. Yuk, B. Lu, S. Lin, K. Qu, J. Xu, J. Luo and X. Zhao, *Nat. Commun.*, 2020, **11**, 1604.
17. C. H. Hsu and F. Mansfeld, *Corrosion*, 2001, **57**, 747-748.
18. T. Li, B. Liang, Z. Ye, L. Zhang, S. Xu, T. Tu, Y. Zhang, Y. Cai, B. Zhang, L. Fang, X. Mao, S. Zhang, G. Wu, Q. Yang, C. Zhou, X. Cai and X. Ye, *Biosens. Bioelectron.*, 2022, **198**, 113855.
19. L. M. Ferrari, U. Ismailov, J.-M. Badier, F. Greco and E. Ismailova, *npj Flexible Electron.*, 2020, **4**, 4.
20. J. Yang, K. Zhang, J. Yu, S. Zhang, L. He, S. Wu, C. Liu and Y. Deng, *Adv. Mater. Technol.*, 2021, **6**, 2100262.
21. X. Niu, X. Gao, T. Wang, W. Wang and H. Liu, *ACS Appl. Mater. Interfaces*, 2022, **14**,

33861-33870.